Study of Vibration Specifications of a Three-axle Truck Using Lagrange Method

Seyed Mohammad Javad Zeidi[*1], Pedram Hoseini[2], Ali Rahmani[3]

[1]PhD Candidate at Florida International University, Department of Mechanical and Material Engineering

[2]MSc student at Amirkabir University of Technology, Department of Mechanical Engineering

[3]Assistant Professor at ShahidRajaeeUniversiy of Tehran, Department of Mechanical Engineering
*Email of Corresponding Author: Szeid001@fiu.edu

Abstract
In this research, Ride quality of a three-axle truck is investigated to understand its vibration specifications and influence of it on special load. The truck is Benz 2624, and the load is rather sensitive to vibrations. The system is considered for an off-road duty. Hence, the vehicle is modeled as a nineteen-degree of freedom system and its equations of motion are derived by employing Lagrange equation. Since, the physical parameters of the vehicle were not available; the truck is modeled in Solidworks CAD software in order to obtain the material and dynamic properties of each component of the truck. Then, a code is developed in MATLAB to calculate natural frequencies and mode shapes of the truck and their corresponding vibrating components in critical speed. A simple model of the truck in ADAMS is employed for validation. The adoption of the results verifies the equations. The developed model can also be used in newer truck with some modifications. It is also necessary to have accurate data for input information in order to change the current model for other utilities.

1. Introduction
Modeling is an important part of engineering. There are two types of the modeling: Physical and numerical. Both types are widely used in engineering [1-8]. Vibration modeling and analyzing are of the application of modeling in engineering. Vibration analysis contributes to improve in many fields and products, e.g., aerospace, automobile, transportation, and so on. The most common goal is unwanted vibration'sidentification and suppression to improve product quality. Multi-axel truck is a real world example, which requires its vibration breakdown.

Generally, vibrations are classified as free and forced vibrations that natural frequencies and mode shapes are the characteristics of the first one [9]. To obtain natural frequencies and mode shapes for damped vibration, two spaces are employed, time domain and frequency domain [10-13]. It is well-known that for a system, undamped and damped natural frequencies are very close particularly in case of vehicles dynamics because of small damping coefficient. Hence, undamped natural frequencies are commonly used to characterize the system [14]. Many approaches have been reported to extract natural frequencies with their own advantages and disadvantages, for instance, Prony method, generalized pencil-of-function method, matrix pencil method, higher order tensor-based method and Newton method [15-22].

Many models such as quarter, bicycle, half and full models of vehicle with different numbers of DoF have been investigated in vehicle dynamics [23-26]. One of the most famous models for vehicles is eight-DoF model, including forward, lateral, yaw and rolling motion plus, four degree of freedom for travel of each wheel [27-28]. Multibody system dynamic models of vehicles have also been proposed in the literature. For instance, RahmaniHanzaki et al. proposed a methodology for dynamic analysis of a multibody system with spherical joints. They considered a suspension system of a vehicle as an example for that [29]. Applying this methodology on a three-axle truck creates the complicated computation. Hence, other people also employed discrete model for the truck. For example, Tabatabaee developed a 16-DoF non-linear model an articulated vehicle, which is validated experimentally [30]. It is also possible to reduce air pollutants specially CO_2 by acquisition of developed model by optimizing several components in the truck [31, 32].

This paper presents a survey on the equations of motion utilizing Lagrange equations to determine natural frequencies and mode shapes of a three-axle truck, i.e., Benz 2624 model. The main purpose is to investigate the influence of dynamics of the vehicle on its load to determine the maximum speed on different paths. Next, a discussion is provided on the results to distinguish the critical DoF using the mode shapes. The developed 19 DoF model can also be applied on many trucks by changing material properties and adding estimations.

2. Modeling the three-axle truck

Using experimental techniques to obtain mass properties of the components of a manufactured vehicle is the most reasonable but very costly. Hence in this work, Solidworks software is employed to model a three-axle truck and to find masses, centers of mass, moments of inertia etc. These physical properties are highly necessary for dynamic simulation of the truck. Figures 1 and 2 show two views of the assembled model of the truck, and some components of the truck, respectively. In this part, the weighty components of the truck such as chassis, tires, differentials, cabin, springs etc. are modeled precisely. Non homogeneous material is assigned to this model since differential consists of several material and precision of properties, which are obtained from this model and are more acceptable.
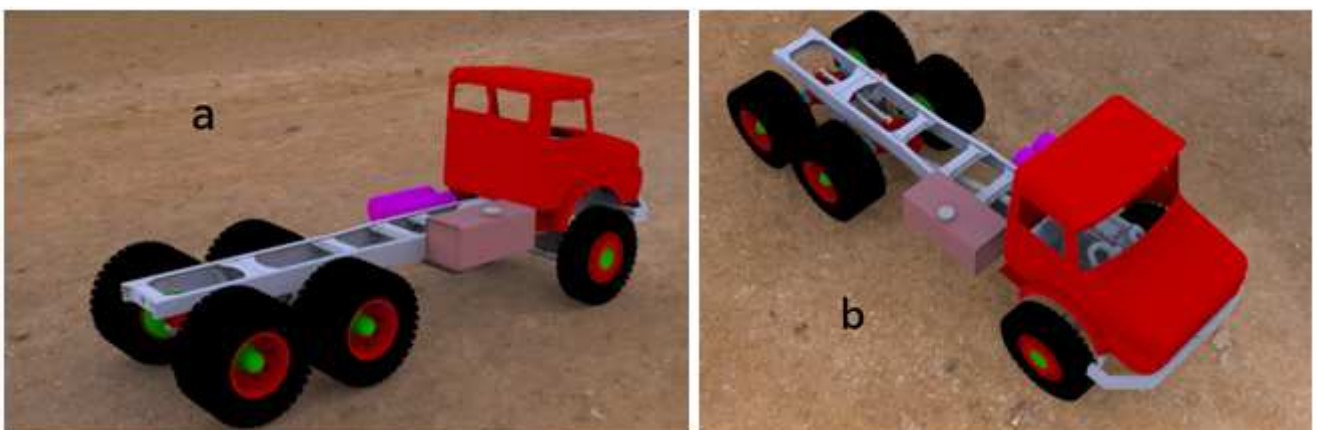

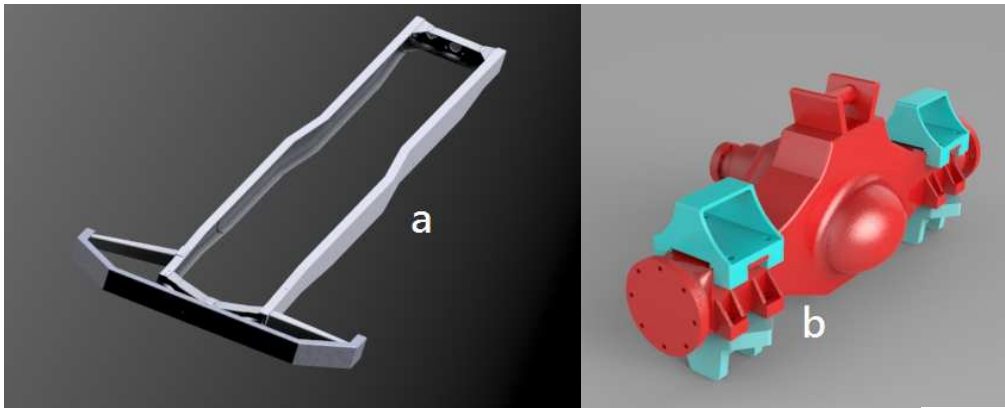Figure1. Two views of the CAD model from the three-axle truck.

Figure2. CAD models of two main components of the truck; a) chassis, b) axle with differential

3. Material Property

Assigning material property to the current model has been very challenging and time consuming. All of the components of truck were modeled separately in order to achieve accurate center of gravity for ADAMS software and initial boundary conditions for MATLAB. Batteries for heavy-duty transport vehicles are so large that the vehicle would barely move, and overhead lines are not practical over millions of acres of farmland, or other off-road logging-trucks, mining trucks, etc., nor could wires be strung over 4 million miles of roads, requiring trucks to have yet another power system after getting off the wires to get to their destination, which doubles the price of the truck. Large, commercial silicon modules convert 17–25% of solar radiation into electricity, and much smaller perovskite cells have already reached a widely reproduced rate of 16–18% in the lab, occasionally spiking higher [33-35]. New Materials for truck can also be assigned to any three axle truck by acquisition of current model.

4. Governing Equations

Lagrange method is utilized to determine dynamic behavior of the mentioned three-axle truck. The truck is considered as a 19-DoF mathematical model. As shown in Figure 3, M_1, M_2 and M_3 are the axles of the truck. Blue springs are considered on behalf of tires, and red springs as leaf springs of the suspensions systems. Also previous mathematical numerical derivation by Zeidi et al. [34-38] has been very useful in this study. Green springs are counted for connecting cabin to the frame and finally, purple spring is used to suspend driver's seat with respect to the cabin. As the rests, W,θ, and φ illustrate displacement, roll, and pitch of the truck in this dynamic analysis. Hence, the 19 DoFs are as follow:

- Driver seat bounce, one degree; w_{106};
- Cab bounce, pitch and roll, three degrees; orderly w_{104}, θ_{104}, φ_{104};
- Chassis bounce (sprung mass), pitch and roll, three degrees; w_{100}, φ_{100}, θ_{100}, respectively:
- Front axle, its bounce and roll, two degrees; orderly w_{101}, θ_{101};
- Intermediate axle, bounce and roll, two degrees; orderly w_{102} , θ_{102};
- Rear axle, bounce and roll, , two degrees; orderly w_{103}, θ_{103};
- 6 bounce motion of the 6 wheels; w_1, w_2, w_3, w_4, w_5, w_6; where w_1 and ; $w_2$are the bounce of left and right steer wheels, respectively; w_3 and $w_4$are the bounce of left and right wheels

of the middle axle, correspondingly; w_5 and w_6 are the bounce of left and right wheels of rear axle, respectively.

The vector of coordinates for the vehicle is written as:

$$W_{19} = [w_{106} w_{104} \theta_{104} \varphi_{104} \ w_{100} \ \theta_{100} \ \varphi_{100} w_{101} \theta_{101} w_{102} \theta_{102} w_{103} \theta_{103} w_1 w_2 w_3 w_4 w_5 w_6]^T \qquad (1)$$
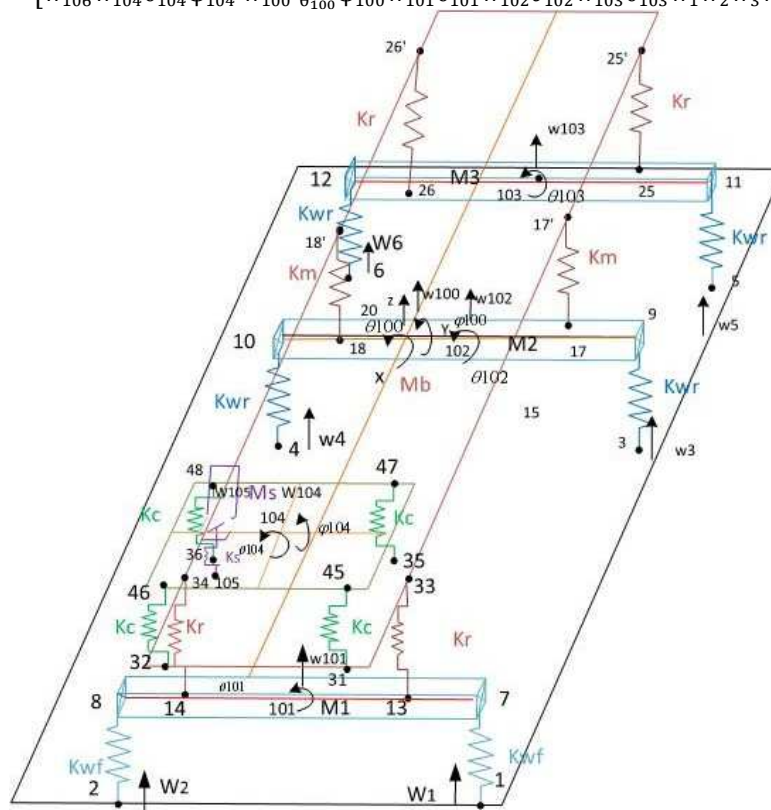

Figure3. The scheme of the 19-DoF model for the truck

Figure 4(a) shows truck model in X-Z plane and distances between different important points. In addition, Figure 4(b) indicates the model in Y-Z plane and the related parameters.
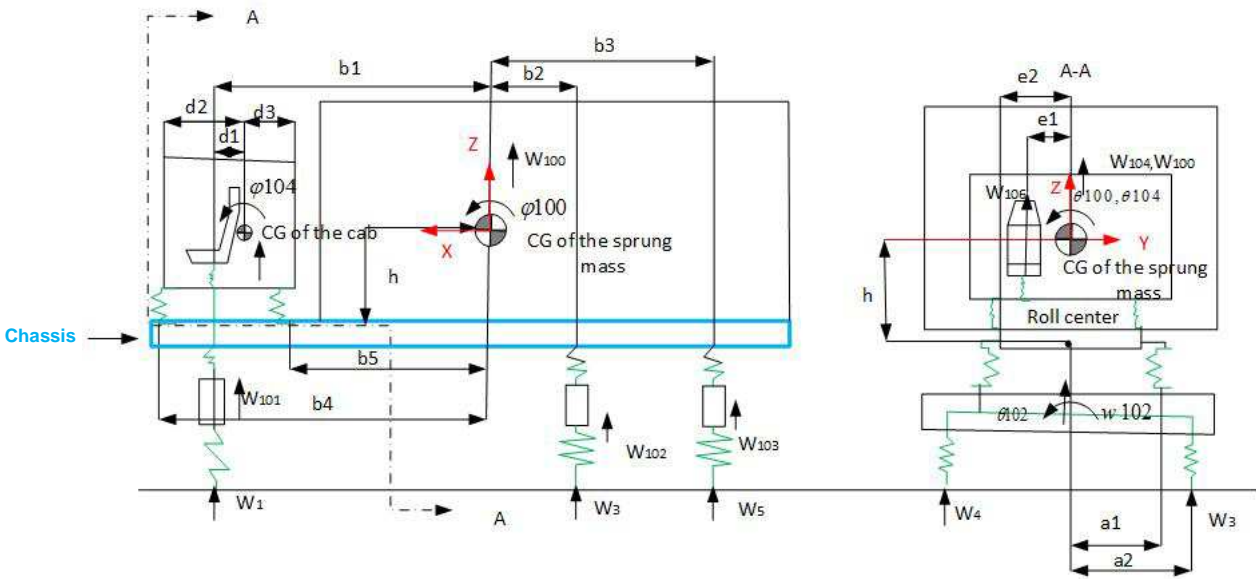
Figure4. CGs (Center of gravity) and other essential parameters of the model

5. Equations of Motion

The Lagrange equation is well-known in the following form for this system:

$$\frac{d}{dt}\left(\frac{dT}{d\dot{W}_{19}}\right) - \left(\frac{dT}{dW_{19}}\right) + \left(\frac{dP}{dW_{19}}\right) = 0$$

(2)

Where, T and P are the kinematic and potential energies of the system respectively.
The kinetic energy of the system is as follow:

$$
\begin{aligned}
T = &\frac{1}{2}M_s(\dot{W}106)^2 + \frac{1}{2}M_c(\dot{W}104)^2 + \frac{1}{2}M_b(\dot{W}100)^2 + \frac{1}{2}M_1(\dot{W}101)^2 + \frac{1}{2}M_2(\dot{W}102)^2 + \frac{1}{2}M_3(\dot{W}103)^2 \\
&+ \frac{1}{2}I_{cx}(\dot{\theta}104)^2 + \frac{1}{2}I_{bx}(\dot{\theta}100)^2 + \frac{1}{2}I_{1x}(\dot{\theta}101)^2 + \frac{1}{2}I_{2x}(\dot{\theta}102)^2 + \frac{1}{2}I_{3x}(\dot{\theta}103)^2 + \frac{1}{2}I_{cy}(\dot{\theta}104)^2 \\
&+ \frac{1}{2}I_{by}(\dot{\theta}100)^2
\end{aligned}
$$

Moreover, the potential energy of the system is obtained as:

$$
\begin{aligned}
P = &\frac{1}{2}K_s(W106 - W105)^2 + \frac{1}{2}K_c(W45 - W31)^2 + \frac{1}{2}K_c(W46 - W32)^2 + \frac{1}{2}K_c(W47 - W35)^2 \\
&+ \frac{1}{2}K_c(W48 - W36)^2 + \frac{1}{2}K_f(W33 - W13)^2 + \frac{1}{2}K_f(W34 - W14)^2 + \frac{1}{2}K_m(W17` - W17)^2 \\
&+ \frac{1}{2}K_m(W18` - W18)^2 + \frac{1}{2}K_r(W25` - W25)^2 + \frac{1}{2}K_r(W26` - W26)^2 + \frac{1}{2}K_{wf}(W7 - W1)^2 \\
&+ \frac{1}{2}K_{wf}(W8 - W2)^2 + \frac{1}{2}K_{wr}(W9 - W3)^2 + \frac{1}{2}K_{wr}(W10 - W4)^2 + \frac{1}{2}K_{wr}(W11 - W5)^2 \\
&+ \frac{1}{2}K_{wr}(W12 - W6)^2
\end{aligned}
$$

By differentiating of T and P with respect to the coordinates and time according to Eq. (2), equations of motion can be organized as:

$$M_{19}\ddot{W}_{19} + K_{19}W_{19} = 0$$

In which M_{19} and K_{19} are orderly mass matrix and stiffness matrix of the 19 DOF of the truck-poster system model. In this equation, $\ddot{W}_{19}$ and $W_{19}$are acceleration vector and displacement vector of the 19 DoF truck-poster system model. In addition, system mass matrix, M_{19} which is a diagonal matrix, is calculated as follow:

$$M_{19} = \text{diag}\left[M_s M_c I_{cx} I_{cy} M_b I_{bx} I_{by} M_1 I_{1x} M_2 I_{2x} M_3 I_{3x} M_{01} M_{02} M_{03} M_{04} M_{05} M_{06}\right]$$

Where, "diag" illustrates that the M_{19} is a diagonal matrix and M_s to M_{06} are located on the main diagonal of the matrix. In this relation, $M_s$andM_c are masses of the seat and the driver, and the cab, respectively; $I_{cx}$and I_{cy} are inertia of the cab about X and Y axes, correspondingly. In the following, M_b, I_{bx}, and I_{by} point to sprung mass, inertia of the sprung mass about X and Y axes, respectively; Also, 1, 2,, and 3 as the indexes in order point to the front axle, middle axle, and the rear axle of the truck. Similarly, M_{01} to M_{06} indicate the masses of the front left to rear right wheels, as well. The 19 nonzero values have been obtained from the truck model in Solidworks software utilizing mass properties. Now, the system stiffness matrix can be written in the following form:

$$K_{19} = \begin{bmatrix} K_{1,1} & K_{1,2} & \cdots & K_{1,19} \\ K_{2,1} & K_{2,2} & & K_{2,19} \\ \vdots & & \ddots & \vdots \\ K_{19,1} & K_{19,2} & \cdots & K_{19,19} \end{bmatrix}$$

The non-zero components of K_{19} are as follows:

$K_{1,1} = K_s$, $K_{1,2} = -K_s$, $K_{1,3} = K_s.e_1$, $K_{1,4} = K_s.d_1$;

$K_{2,1} = -K_s$, $K_{2,2} = 4K_c + K_s$, $K_{2,3} = -K_s.e_1$, $K_{2,4} = K_c(2d_3 - 2d_2) - K_s.d_1$, $K_{2,5} = -4K_c$, , $K_{2,7} = K_c(2b_5 + 2b_4)$;

$K_{3,1} = K_s.e_1$, $K_{3,2} = -K_s.e_1$, $K_{3,3} = 4K_c.e_2{}^2 + K_s.e_1{}^2$, $K_{3,4} = K_s.e_1.d_1$;

$K_{4,1} = K_s.d_1$, $K_{4,2} = -K_s.d_1 - 2K_c.d_2 + 2K_{c3}.d_3$, $K_{4,3} = K_s.d_1.e_1$, $K_{4,4} = K_s.d_1{}^2 + 2K_c(d_2{}^2 + d_3{}^2)$, $K_{4,5} = 2K_c(d_2 - d_3)$, $K_{4,6} = -2K_c.d_3.e_2$, $K_{4,7} = -2K_c.d_2.b_4 + 2K_c.d_3.b_5$;

$K_{5,2} = -4K_c$, $K_{5,4} = -2K_c.d_3$ $K_{5,5} = 2K_f + 2K_m + 2K_r + 4K_c$, $K_{5,6} = 2(K_f + K_m + K_r).a_1 + 2K_c.e_2$, $K_{5,7} = -2K_f.b_1 + 2K_m.b_2 + 2K_r.b_3 - 2K_c.b_4$, $K_{5,8} = -2K_f$, , $K_{5,10} = -2K_m$, $K_{5,11} = 2K_m.a_1$ $K_{5,12} = -2K_r$;

$K_{6,2} = -2K_c.e_2$, $K_{6,3} = -2K_c.e_2{}^2$, $K_{6,4} = -2K_c.e_2.d_3$, $K_{6,5} = 2(K_f + K_m + K_r).a_1 + 2K_c.e_2$, $K_{6,6} = 2(K_f + K_m + K_r).a_1{}^2 + 4K_c.e_2{}^2$, $K_{6,7} = -2K_f.a_1.b_1 - 2K_m.a_1.b_2 + 2K_r.a_1.b_3 - 2K_c.e_2.b_4$, $K_{6,8} = -2K_f.a_1$, , $K_{6,12} = -2K_r.a_1$;

$K_{7,2} = 4K_c.b_4$, $K_{7,4} = -2K_c.b_4.d_2 + 2K_c.b_5.d_3$, $K_{7,5} = -2K_f.b_1 + 2K_m.b_2 + 2K_r.b_2 - 2K_c.b_4 - 2K_c.b_5$, $K_{7,6} = -2K_f.a_1.b_1 + 2K_5.a_1.b_3 + 2K_c.e_2.b_4$, $K_{7,7} = 2K_f.b_1{}^2 + 2K_m.b_2{}^2 + 2K_r.b_3{}^2 + 2K_c.b_4{}^2 + 3K_c.b_5{}^2$, $K_{7,8} = 2K_f.b_1$, $K_{7,10} = -2K_m.b_2$, $K_{7,11} = 2K_m.b_2.a_1$, $K_{7,12} = -2K_r.b_3$;

$K_{8,6} = -2K_f.a_1$, $K_{8,7} = 2K_f.b_1$, $K_{8,8} = 2K_f + 2K_{wf}$;

$K_{9,9} = 2K_{wf}.a_2{}^2 + 2K_1.a_1{}^2$ $K_{9,14} = -K_{wf}.a_2$, $K_{9,15} = K_{wf}.a_2$;

$K_{10,5} = -2K_m$, $K_{10,6} = -2K_m.a_1$, $K_{10,7} = -2K_3.b_2.$, $K_{10,10} = 2K_{wr}$, $K_{10,11} = -2K_3.a_1$, $K_{10,16} = -K_{wr}$, $K_{10,17} = -K_{wr}$;

$K_{11,5} = 2K_m.a_1$, $K_{11,7} = 2K_m.b_2.a_1$, $K_{11,10} = -2K_m.a_1$, $K_{11,11} = 2K_m.a_1{}^2 + 2K_{wr}.a_2{}^2$, $K_{11,16} = -K_{wr}.a_2$, $K_{11,17} = K_{wr}.a_2$;

$K_{12,5} = -2K_r$, $K_{12,6} = -2K_5.a_1$, $K_{12,7} = -2K_r.b_3$, $K_{12,12} = 2K_{wr}$, , $K_{12,18} = -2K_{wr}$;

$K_{13,13} = 2K_{wr}.a_2{}^2 + 2K_5.a_1{}^2$, $K_{13,18} = -K_{wr}.a_2$, $K_{13,19} = -K_{wr}.a_2$;

$K_{14,8} = -K_{wf}$, $K_{14,9} = -K_{wf}.a_2$, $K_{14,14} = K_{wf}$;

$K_{15,8} = -K_{wf}$, $K_{15,9} = K_{wf}.a_2$, $K_{15,15} = K_{wf}$;

$K_{16,10} = -K_{wr}$, $K_{16,11} = -K_{wr}.a_2$, $K_{16,16} = K_{wr}$;
$K_{17,10} = -K_{wr}$, $K_{17,11} = K_{wr}.a_2$, $K_{17,17} = K_{wr}$;
$K_{18,12} = -K_{wr}$, $K_{18,13} = K_{wr}.a_2$, $K_{18,18} = K_{wr}$;
$K_{19,12} = -K_{wr}$, $K_{19,13} = -K_{wr}a_2$, $K_{19,19} = K_{wr}$;

In which, K_s is the stiffness of spring of driver seat; K_c is the stiffness of each spring of cab suspension; K_f is the stiffness of each spring of front axle suspension; K_m, and K_r are defined for stiffness of every spring for the middle axle and the rear axle, respectively; K_{wf} is also considered for the equivalent stiffness of each of front tires, while K_{wr} plays the same role for the tires of middle and rear wheels. Other variables and constants were illustrated in the previous sections.

6. Validation
ADAMS software has provided a unique environment for dynamic modeling of multibody systems. Here, we utilize the software to validate the equations of motion for the truck. For this purpose, one of the modules of this software, i.e., ADAMS/Truck, is employed. The three-axle truck model, which is available in the software, is utilized and the characteristics of the truck are entered. The truck, as a vibrational system is moved on a sinusoidal road to excite the model with a wide range of frequencies as shown in Figure 5. Times, in which the accelerations of the CG are more than their neighborhood, can be used to find natural frequencies using constant acceleration of the truck. Figure 6 shows accelerations obtained from this procedure.
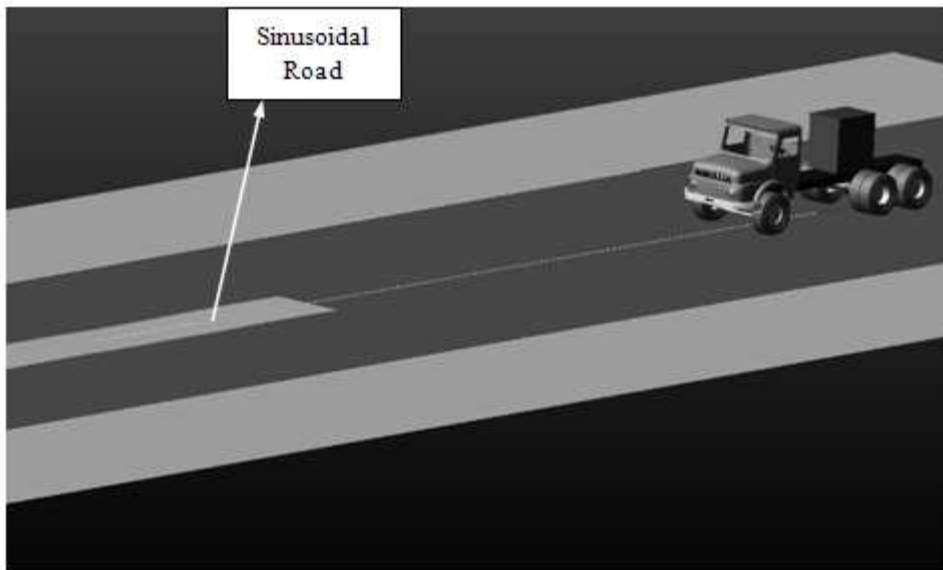

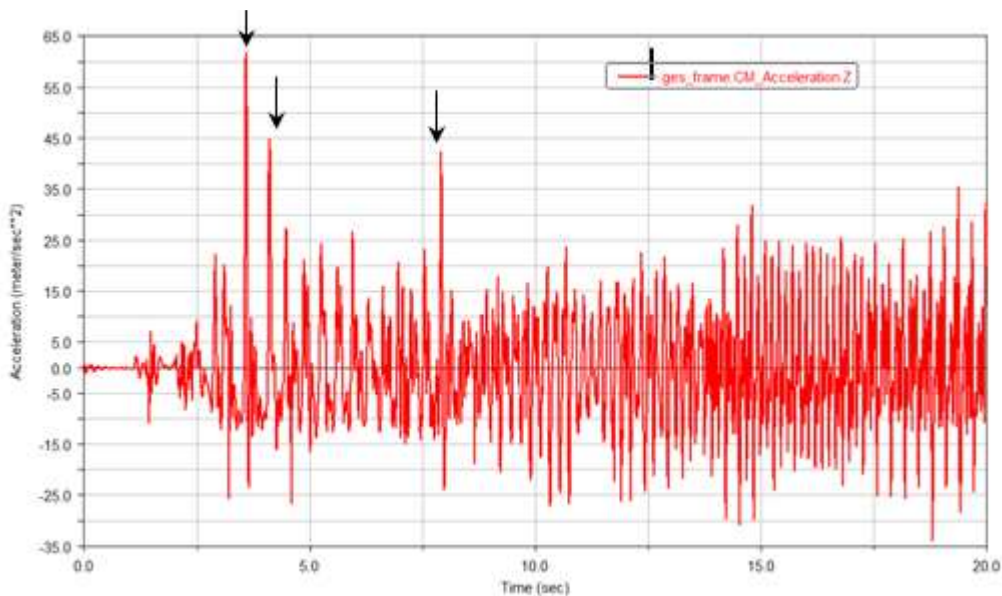Figure5. Calculating truck dynamic characteristics using ADAMS

Figure6. Acceleration for the truck in ADAMS

To verify the accuracy of the results, some of the natural frequencies, which are derived from MATLAB code, are compared with the simulation results from ADAMS software as shown in table 1. Comparing two or three natural frequencies of the system with those obtained from analytical procedure replies that the formulation is valid.

Table1. Comparison of natural frequency which is obtained in MATLAB and ADAMS

Dominant motion	Natural frequency(rad/s) (Analytically)	Natural frequency(rad/s) (ADAMS)	Difference (%)
Right steer wheel bounce	77.1316	83.1044	7.18
Rear axle bounce	103.358	90.1399	12.78
Center axle bounce	265.249	261.174	1.56

7. Natural frequencies and corresponding mode shapes

To determine the natural frequencies of the system, the free vibration of the system is considered. The equations of motion for free vibration were derived in eq. 5. The characteristic equation of the system is arisen from eq. 5 and Eigen values of the characteristic equation are natural frequencies of the system. Eigenvectors of the equation are utilized to find natural frequency corresponding to each DOF.

Table 2 shows, natural frequencies and mode shapes for the 19 DOF truck. For each natural frequency, there is a 19×1 vector of mode shape. Among the elements of every mode shape, the highest value shows dominant motion. Dominant motion is the most intense motion in each natural frequency.

Table2. Natural frequency, mode shape and dominant motion

Natural frequency(rad/s)	Dominant motion
0.000004622358	right rear steer wheel bounce
0.000003451677	right steer wheel bounce
0.000000001065513	left rear steer wheel bounce
0.011396794116965	Deriver seat bounce
0.022510398030284	Cab roll
0.032668119888841	Cab bounce
50.670520926536	right rear steer wheel bounce
51.637956185048	left center steer wheel bounce
64.379923963352	left center steer wheel bounce
66.626459703922	Cab roll
70.244931281563	Left steer wheel bounce
77.136046229719	Right steer wheel bounce
103.358018471211	Rear axle bounce
189.294739253455	Center axle roll
189.588958526633	Center axle roll
265.249162539134	Center axle bounce
586.273194921182	Steer axle bounce
596.770119450067	Steer axle roll
1133.920811119840	Steer axle bounce

8. Natural frequency using 16 DoF model

In general, the DOF of the driver seat and the cab of the truck are not considered. To investigate the influence of this withdrawal, by excluding three degrees of freedom – driver seat bounce, cab bounce and cab roll- a 16 DOF model is provided and solved. Hence, three dominant motions from three different ranges are opted to compare from those that were obtained from 19 DOF model. According to table 3, by eliminating some degrees of freedom, natural frequencies aggravate. Comparing the results reports about 10% error in natural frequencies.

Table 3. Natural frequencies using 16 DoF model for three dominant motions

Natural frequency(rad/s)	Dominant motion	Error
53.874560935562	right rear steer wheel bounce	6.3%
201.494719652476	Center axle roll	6.5%
1250.354821459930	Steer axle bounce	10.4%

9. Calculation of the Suspension Static Deflection and the Reaction Force on Each Wheel

The suspension static displacement which is the relative displacement of the two ends of the suspension can be obtained as following (for instance we have just mentioned seat and cab static displacement formula in which the subscripts are f = front, r=right, l = left, re = rear):

$$d_{seat} = w_{106} - w_{105} = w_{106} - (w_{104} - d_1\theta_{104} - e_1\phi_{104})$$

$$d_{cab_{fl}} = w_{45} - w_{31} = (w_{104} + e_2\theta_{104} - d_2\phi_{104}) - (w_{100} + e_2\theta_{100} - b_4\phi_{100})$$
$$d_{cab_{fr}} = w_{46} - w_{32} = (w_{104} - e_2\theta_{104} - d_2\phi_{104}) - (w_{100} - e_2\theta_{100} - b_4\phi_{100})$$
$$d_{cab_{re_l}} = w_{47} - w_{35} = (w_{104} + e_2\theta_{104} + d_3\phi_{104}) - (w_{100} + e_2\theta_{100} - b_5\phi_{100})$$
$$d_{cab_{re_r}} = w_{48} - w_{36} = (w_{104} - e_2\theta_{104} + d_3\phi_{104}) - (w_{100} - e_2\theta_{100} - b_5\phi_{100})$$

The displacements of all degrees of freedom that have been used above have been calculated by considering the gravity.

Hence, the static deflection of each suspension spring member is listed below:

Table4. Deflection of suspension springs.

	Seat	Cab, front left	Cab, front right	Cab, rear left	Cab, rear right	
Static Deflection (m)	-0.0594	-0.0088	-0.0212	-0.0092	-0.0216	
	Main, steer left	**Main, steer right**	**Main, center left**	**Main, center right**	**Main, rear left**	**Main, rear right**
Static Deflection (m)	-0.1875	-0.1895	-0.1456	-0.1488	-0.1173	-0.1204
	Tire, steer left	**Tire, steer right**	**Tire, center left**	**Tire, center right**	**Tire, rear left**	**Tire, rear right**
Static Deflection (m)	-0.031	-0.0311	-0.0348	-0.0351	-0.0279	-0.0282

And the reaction force on each wheel can be obtained by considering tire stiffness; hence result for the reaction force calculation is listed in the following table:

Table5. Calculation of reaction force

	Tire, steer left	Tire, steer right	Tire, center left	Tire, center right	Tire, rear left	Tire, rear right
Reaction force (N)	21399	21483	48102	48531	38525	38954

It is clearly seen that wheels on the right side are subject to slightly greater loads than those on the left side consistent with the chassis and cab lean. This effect results from the offset position of the driver seat.

10. Conclusion

A 19-DoF system had been chosen in order to study the dynamic characteristics of a three-axle truck. Physical properties are calculated using a model in Solidworks CAD software. Lagrange equations are used for deriving equations of motion. Validation performed by comparison of data achieved analytically and those resulted from ADAMS simulation, which replies the accuracy of the formulation. Finally, natural frequencies, mode shapes and dominant motions have been observed. In each natural frequency, a 19-dimensional mode shape is established, which is useful to know the vibrating component of the truck. Finally, the influence of elimination of three non-prominent DOFs is investigated. The results illustrate that the equations of motion obtained in this work can

increase the accuracy by 10%. It was also found that right side wheels of the truck experience more intense load in comparison with the left side wheels due to chassis and cab lean.

11.References

[1] Rahmani, A., Mirmohammadi, A., Zeidi, SMJ. and Shojaei, S., 2015. Numerical Approach toward Calculation of vibration Characteristics of the Multi Axles Truck Using Lagrange Method", Journal of Modern Processes in Manufacturing and Production. 4(1):57-64.

[2] Shojaei S., Zeidi, SMJ. and Mirmohammadi A. 2015. Analytical Analysis Approach to Study of the Vibration Characteristics of the Multi Axles Truck and its Validation. Proceedings of the International Conference in New Research of Industry and Mechanical Engineering.

[3] Hamedi, A., Malekmohammadi, I., Mansoori, A., and Roshanaei, H. 2012. Energy Dissipation in Stepped Spillway Equipped with Inclined Steps Together with End Sill. Fourth International Conference on Computational Intelligence and Communication Networks. IEEE.

[4] Hamedi, A. and Fuentes, H.R. 2016. New Relationship between a Vertical Gate Opening and Downstream Flow Stability: Experimental Development. World Environ. World Environmental and Water Resources Congress.

[5] Hamedi, A. and Fuentes, H.R. 2015. Comparative Effectiveness and Reliability of NEXRAD Data to Predict Outlet Hydrographs Using the GSSHA and HEC-HMS Hydrologic Models. World Environmental and Water Resources Congress.

[6] Hamedi, A., Hajigholizadeh, M., and Mansoori, A. 2016. Flow Simulation and Energy Loss Estimation in the Nappe Flow Regime of Stepped Spillways with Inclined Steps and End Sill: A Numerical Approach. Civil Engineering Journal. 2(9):426-437.

[7] Hamedi, A. and Ketabdar, M. 2016. Energy Loss Estimation and Flow Simulation in the skimming flow Regime of Stepped Spillways with Inclined Steps and End Sill: A Numerical Model. International Journal of Science and Engineering Applications.5(7):399-407.

[8] Ketabdar, M. and Hamedi, A. 2016. Intake Angle Optimization in 90-degree Converged Bends in the Presence of Floating Wooden Debris: Experimental Development. Florida Civil Engineering Journal. 2:22-27.

[9] Rao, S. S.and Yap, F. F. 1995. Mechanical Vibrations, Addision-Wesley Publishing Co. United States of America.

[10] Tse,F. S., Morse, I. E. and Hinkle, R. T. 1976. Mechanical Vibration: Theory and Applications, 2nd Edition. Allen and Bacon, Inc, Boston.

[11] Dimarogonas, A. D. 1975. Vibration Engineering, West Publishing Co., Inc., New York.

[12] Meiroritch, L. 1967. Analytical Methods in Vibrations, Macmillan Publishing Co., Inc, New York.

[13] Timoshenko, S., Young. D. H. and Weaver, W. 1974. Vibration Problems in Engineering, 4th Edition, John Wiley& Sons, Inc., New York.

[14] Wong, J, Y. 2001. Theory of Ground Vehicles, 3rd Edition, John Wiley& Sons, Inc., New York.

[15] Kumaresan, R., Tufts D. W. and Scharf L. L. 1984. A prony method fornoisy data: Choosing the signal components and selecting the order in exponential signal models. Proc. IEEE, 72:230–233.

[16]   Hua, Y. and Sarkar T. K. 1989. Generalized pencil-of-function method for extracting poles of an em system from its transient response. IEEE Trans. Antennas Propag. 37: 229–234.

[17]   Hua, Y. and Sarkar, T, K.1990. Matrix pencil method for estimating parameters of exponentially damped/undamped sinusoids in noise," IEEE Trans. Acoust., Speech, Signal Process. 38:814–824.

[18]   Pisarenko, Y. F.1973.The retrieval of harmonics from a covariance function.Geo. Phys. J. Roy. Astron. Soc. 33:347–366.

[19]   Djermoune E, H. and Tomczak, M. 2009.Perturbation analysis of subspacebased methods in estimating a damped complex exponential. IEEE Trans. Signal Process. 57: 4558–4563.

[20]   Boyer, R., Lathauwer, L. and Abed-Meraim, K. 2007. Higher order tensor-based method for delayed exponential fitting. IEEE Trans. Signal Process. 55:2795–2809.

[21]   Boyer, R., and Abed-Meraim, K., 2007. Asymptotic performance for delayed exponential process. IEEE Trans. Signal Process. 55: 3139–3143.

[22]   Lee, J, H. and Kim, H, T. 2010. Application of Newton Method to Natural Frequency Estimation. IEEE, 58: 212-214.

[23]   Wong. J, Y. 2001.Theory of ground vehicles. John Wiley & Sons, Canada.

[24]   Jazar, R. 2013. Advanced Vibrations:A modern Approach. Springer, New York.

[25]   Jazar, R. 2010. Vehicle Dynamics: Theory and Application. Springer, New York.

[26]   Gillespie, T, D.1992. Fundamentals of Vehicle Dynamics. SAE publishing group, United States of America.

[27]   Yang, X., Zengcai, W. and Weili, P. 2009. Coordinated Control of AFS and DYC for Vehicle Handling and Stability Based on Optimal Guaranteed Cost Theory. Vehicle System Dynamics. 47:57-79.

[28]   Zheng, S., Tang, H., Han, Z. and Zhang, Y.2006.Controller Design for Vehicle Stability Enhancement," Control Engineering Practice.14:1413-1421.

[29]   A. Rahmani-Hanzaki, S. K. Saha and P. V. M. Rao.2009. An improved recursive dynamic modeling of a multibody system with spherical joint, International Journal of Multibody system dynamics. 21:325-345.

[30]   Tabatabaee, S,H. 2013. Integrated control to improve directional stability and maneuverability of the articulated heavy vehicle, PhD Thesis, K. N. Toosi University of Technology Faculty of Mechanical Engineering.

[31]   Darvish, S., Gopalan, S., and Zhong, Y.2016.Thermodynamic Stability Maps for the $La_{0.6}Sr_{0.4}Co_{0.2}Fe_{0.8}O_{3\pm\delta}$–$CO_2$–$O_2$ System for Application in Solid Oxide Fuel Cells. Journal of Power Sources. 336:351–359.

[32]   Darvish, S., Saxena, SK., Zhong, Y. 2015. Quantitative Analysis of $(La_{0.8}Sr_{0.2})_{0.98}MnO_{3\pm\delta}$ Electronic Conductivity Using CALPHAD Approach. The 39th International Conference on Advanced Ceramics and Composites (ICACC).

[33]   Darvish, S., Karbasi, A., Saxena SK. and Zhong Y, 2015. Weight Loss Mechanism of $(La_{0.8}Sr_{0.2})_{0.98}MnO_{3\pm\delta}$During Thermal Cycles. The 39th International Conference on Advanced Ceramics and Composites (ICACC).

[34]   Zeidi, SMJ. and Mahdi, M. 2015. Evaluation of the physical forces exerted on a spherical bubble inside the nozzle in a cavitating flow with an Eulerian/Lagrangian approach, European Journal of Physics, 36(6):41-65.

[35]   Zeidi, SMJ. and Mahdi. M. 2014. Investigation of viscosity effect on velocity profile and cavitation formation in Diesel injector nozzle. Proceedings of the 8th International Conference on Internal Combustion Engines.

[36]   Zeidi, SMJ., and Mahdi, M. 2015. Effects of nozzle geometry and fuel characteristics on cavitation phenomena in injection nozzles. Proceedings of the 22st Annual International Conference on Mechanical Engineering-ISME.

[37]   Zeidi, SMJ and   Mahdi, M. 2015. Investigation effects of injection pressure and compressibility and nozzle entry in Diesel injector nozzle's flow. Journal of Applied and Computational Mechanics. 1(2):83–94.

[38]   Zeidi, SMJ., Dulikravich, G., S., and Reddy, Sohail, R. 2017. Effects of needle lift and fuel type on cavitation formation and heat transfer inside diesel fuel injector nozzle. Proceedings of 17th International Symposium on Advances in Computational Heat Transfer.